Aerodynamic Characteristics of Crescent and Elliptic Wings at High Angles of Attack

C. P. van Dam*
University of California, Davis, Davis, California
P. M. H. W. Vijgen†
High Technology Corporation, Hampton, Virginia
and
B. J. Holmes‡
NASA Langley Research Center, Hampton, Virginia

Static longitudinal- and lateral-directional forces and moments were measured for an elliptic- and crescent-wing model in the NASA Langley Research Center 14 × 22 ft subsonic tunnel for an angle-of-attack range that included stall and poststall conditions and at a Reynolds number of about 1.8×10^6, based on the average wing chord. The force and moment data and the flow-visualization results indicated that the crescent-wing model, with its highly swept tips, produced better high angle-of-attack aerodynamic characteristics than the unswept elliptic model. Leading-edge separation-induced vortex flow over the highly swept tips is thought to produce this improved behavior. The design concept of combining vortex flow over the outboard wing portion at high angles of attack and attached flow over the entire wing at cruise/climb conditions should result in safer and more efficient airplanes.

Nomenclature

AR = aspect ratio, $= b^2/S$
b = wing span, ft
C_L = lift coefficient, $=$ lift/$(q_\infty S)$
$C_{L,\alpha}$ = lift-curve slope, $= \partial C_L/\partial\alpha$, deg^{-1}
C_l = rolling-moment coefficient, = rolling moment/$(q_\infty Sb)$
C_m = pitching-moment coefficient, = pitching moment/$(q_\infty Sc_{av})$
$C_{m,\alpha}$ = slope of pitching-moment coefficient curve, $= \partial C_m/\partial\alpha$, deg^{-1}
C_n = yawing-moment coefficient, = yawing moment/$(q_\infty Sb)$
c = chord length, ft
c_{av} = average chord length, $= S/b$, ft
c_l = sectional lift coefficient
c_r = root chord length, ft
q_∞ = freestream dynamic pressure, lb/ft^2
S = wing area, ft^2
U = freestream velocity, ft/s
y = spanwise distance from wing root, ft
α = angle of attack, deg
β = sideslip angle, deg
η = nondimensional spanwise station, $= y/(b/2)$

Received Jan. 6, 1990; presented as Paper 90-0300 at the AIAA 28th Aerospace Sciences Meeting, Reno, NV, Jan. 8–11, 1990.

*Associate Professor, Department of Mechanical, Aeronautical and Materials Engineering. Member AIAA.
†Research Scientist. Member AIAA.
‡Acting Deputy Director for Aeronautics. Associate Fellow AIAA.

Introduction

IN 1971, Küchemann[1] discussed the possibility of designing wings that combine vortical flows with classical attached flows. Although he admitted that "such designs must be more risky and are more likely to fail,"[2] Küchemann suggested that the benefits justified abandonment of the classical concept of maintaining attached flow over the entire wing throughout the whole flight regime. This idea of combined vortex flows and classical attached flows has been integrated in the wing design of highly maneuverable military aircraft; all current generation fighter aircraft make use of this concept in one way or the other. However, in the design of low-speed and transport aircraft, the concept of maintaining attached flow over the entire wing throughout the flight regime (from cruise to near stall) has still been followed. In this philosophy, flow separation is avoided, sometimes at great cost, until angles of attack are close to stall, when trailing-edge separation is designed to occur over the inboard portion of the wing. The outboard region of the wing is designed to maintain attached flow until poststall angles of attack to maximize roll stability and control and to minimize the chances of stall-spin entry.

To meet these design objectives in the framework of the classical attached-flow approach, several options are available. First, wing sweep is kept to a minimum to reduce tip loading and, thus, the danger of tip stall. Conventional aft sweep puts the outboard portion of the wing in the upwash field of the inner part of the wing and, as a result, the outer part is at higher effective angle of attack than the inner part. However, flow separation over the tip region must be minimized; therefore, the wing is swept only as required to minimize the compressibility drag rise at cruise conditions. Wing twist can also be used to reduce the aerodynamic loading over the outboard portion of a swept or unswept wing. However, a significant induced-drag penalty at cruise often results because of deviations from an optimal spanwise-load distribution. Wing section shape can be varied in the spanwise direction with high $c_{l,max}$ profiles employed in the outer wing region. This design option may result in a viscous drag penalty at cruise conditions because airfoil performance at these conditions is sacrificed. Finally, wing leading-edge mod-

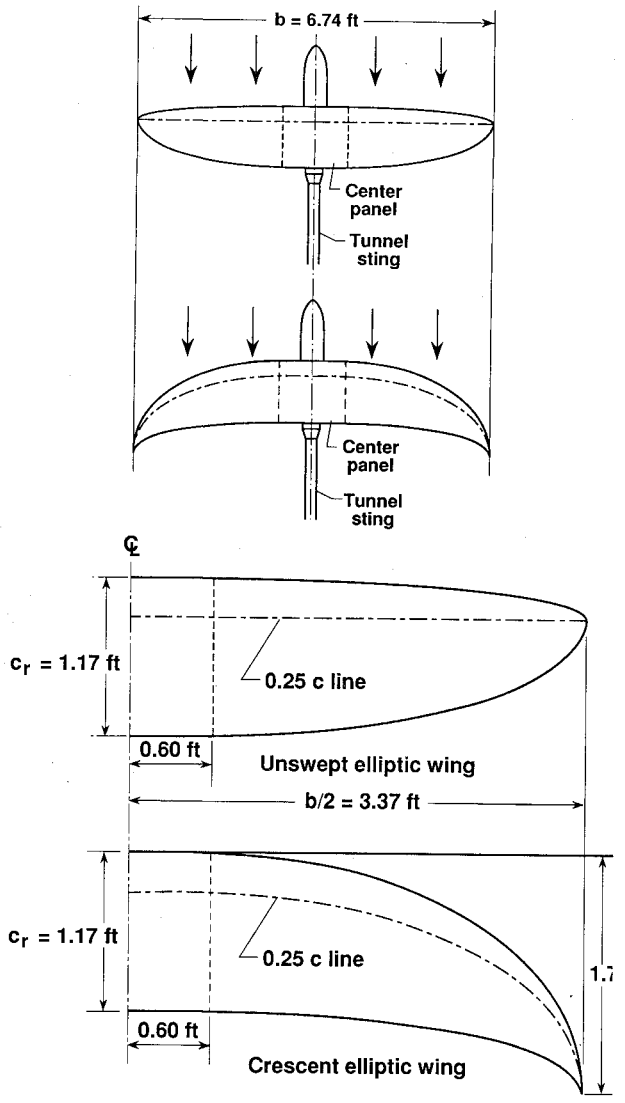

Fig. 1 Planform geometry of crescent and elliptic wind-tunnel models.

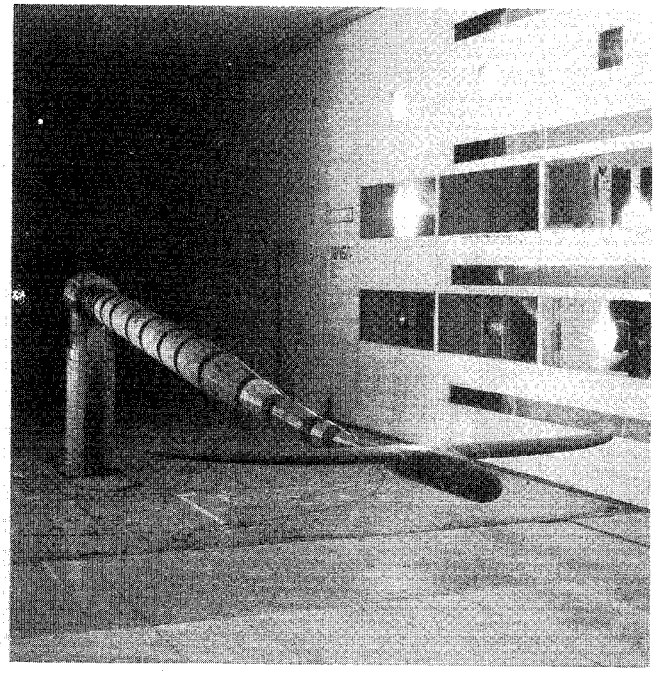

Fig. 2 Photo of crescent model in test section of the 14 × 22 ft subsonic tunnel.

ifications such as slots, slats, or flaps can be incorporated to improve the aerodynamic characteristics at high angle of attack. These systems often result in increased complexity, maintenance, cost, and sometimes degraded aerodynamic cruise performance. In recent years, the fixed outboard leading-edge droop has proven to significantly increase the stall departure and spin resistance of low-speed aircraft.[3] But this simple modification may reduce the aerodynamic performance at cruise conditions. Also, for wings with a relatively blunt leading edge or for high aspect ratio wings, a leading-edge droop is not always effective to increase stall departure and spin resistance.

In this paper, a crescent-wing planform that combines attached flow over the entire wing at moderate angles of attack with vortical flow over the outboard portion at near stall is examined experimentally. Wing sweep is used to induce

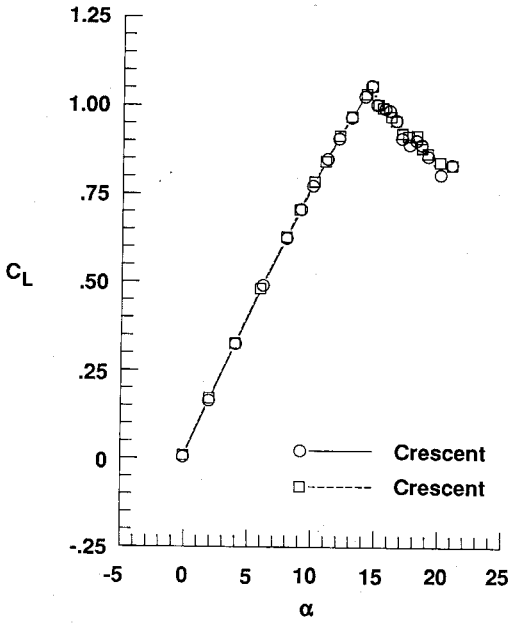

a) Lift curve (α = 0–21 deg)

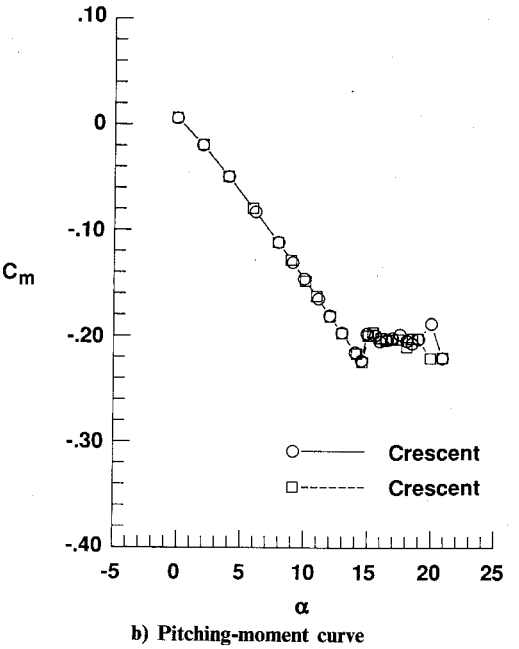

b) Pitching-moment curve

Fig. 3 Comparison of results for two separate data runs (crescent model).

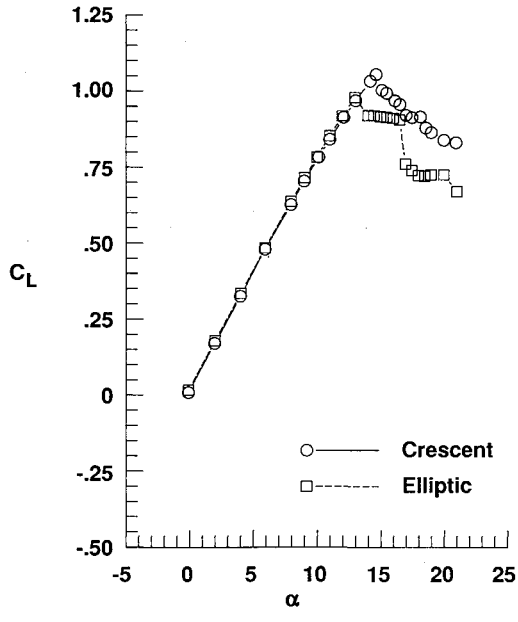

a) $\alpha = 0-21$ deg

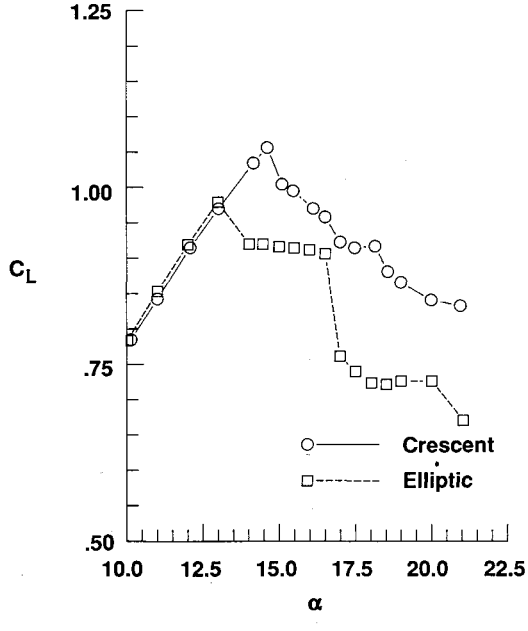

b) $\alpha = 10-21$ deg

Fig. 4 Lift curves of elliptic and crescent model.

separation along the rounded leading edge of the outboard wing region at high angles of attack. The resulting vortical flow over this portion of the wing produces a significant amount of local lift and, consequently, should improve lateral stability and controllability at stall and poststall conditions. Also, the wingtip with vortex flow tends to generate a stabilizing nose-down pitching moment at stall. However, at cruise and climb conditions, the flow must remain attached over the entire wing to minimize drag. It should be noted that this concept of a highly swept tip can also be beneficial for wings of high-speed airplanes[4] and rotor blades of helicopters.[5] A wind-tunnel program was conducted to evaluate this design concept for moderate-to-high aspect ratio wings, first introduced in Ref. 6 (also see Ref. 7). The crescent shape was originally developed to investigate the lift-dependent drag characteristics of this type of wing and is a further development of wings with discontinuously sheared tips.[6,8] The lift and the moment characteristics (Part I of the program) are reported in this paper, whereas the drag characteristics (Part II) are reported in Ref. 9.

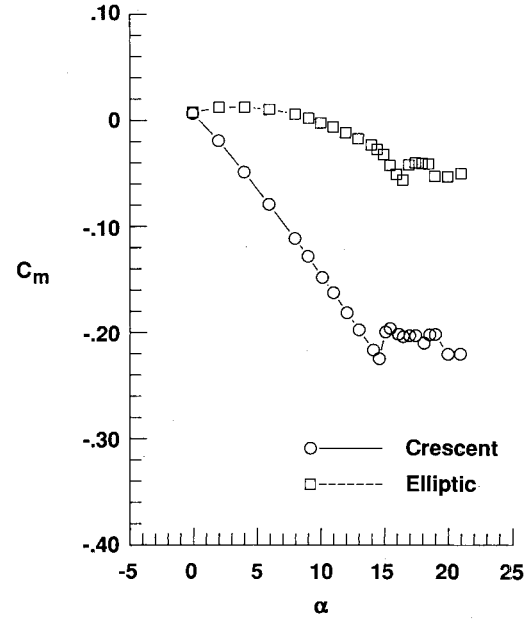

Fig. 5 Pitching-moment data of elliptic and crescent model.

Experiment

The wind-tunnel program was conducted in the NASA Langley Research Center 14 × 22 ft subsonic tunnel to investigate the influence of wing planform shape on the high-angle-of-attack aerodynamic characteristics. In Fig. 1, a plan view is shown of the elliptic- and the crescent-wing configurations investigated. Figure 2 provides a photograph of the model and the sting mount used in the present test. Both wings had identical wing area ($S = 6.47$ ft^2), wing span ($b = 6.74$ ft), spanwise chord distribution (constant for center panel and elliptic for outboard panel), aspect ratio ($AR = 7.014$), and airfoil section shape in the freestream direction. Also, the models had zero wing twist and zero dihedral. The only difference between the two models was the planform shape. The crescent wing had a quarter-chord line that is curved rearward, whereas the elliptic wing had a straight, unswept quarter-chord line. The center body and the center wing panel (see Fig. 1) were obtained from an existing model.[10] This dictated the root chord length and the NACA 0012 section shape for the outboard wing panel.

The dynamic pressure, unit Reynolds number, and Mach number of the freestream during the measurements were approximately 100 lb/ft^2, 1.85×10^6/ft, and 0.27, respectively. For the average chord of slightly less than 1 ft, a test Reynolds number of 1.8×10^6 was realized. The rounded leading edge of the wing maximizes the leading-edge suction force and, thus, the performance at cruise and climb conditions with attached flows. The separation-induced vortex flow is very much Reynolds number dependent for wings with rounded leading edges.[11] The achieved Reynolds number approached the range of Reynolds numbers encountered by low-speed aircraft at high lift coefficients. The force-and-moment measurements for both configurations were obtained with a six-component balance mounted in the model center body (Fig. 1). This balance was sized to handle the static and the dynamic loads at stall and poststall conditions. Consequently, the accuracy of the drag measurements was significantly reduced.[10] A much smaller three-component balance was used to measure the drag characteristics of both wings for angles of attack below stall. The results of this part of the test program are presented in Ref. 9.

Boundary-layer transition was fixed on both models at 5% of the chord (in the freestream direction) over the upper and lower surfaces along the entire span. The width of the trip strips was 0.125 in. Over the crescent-wing model, attachment-line trip strips were located around the leading edge at

about $\eta = \pm 0.98$. These trips were oriented normal to the leading edge to induce transition of the leading-edge attachment-line boundary layer along the highly swept tips at low angles of attack.[12] On the center body, the transition was fixed circumferentially at 3.0 in. downstream of the nose.

The models were tested for an angle-of-attack range from 0 to 21 deg (tunnel constraint) at zero sideslip angle. Also, force and moment measurements were made for an angle-of-sideslip variation from 0 to 15 deg, 15 to −15 deg, and −15 to 0 deg at several angles of attack. Windoff tares were carefully determined for each configuration. The analog data signals were low-pass filtered (7.5 Hz) to remove the effects of model and tunnel vibrations and dynamic-pressure fluctuations. At each incidence angle, balance readings were taken over a period of 10 s at a rate of 5 data-sampling cycles/s. In the following figures, each experimental datum point represents the average value of these readings. The repeatability of the data is exemplified by the comparisons shown in Fig. 3; lift- and pitching-moment results obtained during two separate data runs are compared. The comparisons of the data demonstrate good repeatability even at stall and poststall conditions.

Surface oil flow visualizations were conducted to study the behavior of the boundary layer. A mixture of light oil and titanium dioxide was used to visualize the surface streak lines. The visualizations were conducted at the test Reynolds number and at several angles of attack.

Results

In this section, the effects of wing planform on high angle of attack behavior are illustrated by comparing the lift and the static-stability characteristics and the flow visualizations for both configurations. The moments were measured with respect to a fixed point on the model center line, located longitudinally and vertically at the $0.25c_r$ location (3.5 in. aft of the leading edge). The lateral-directional moments were referred to the body-axis system with the origin located at the

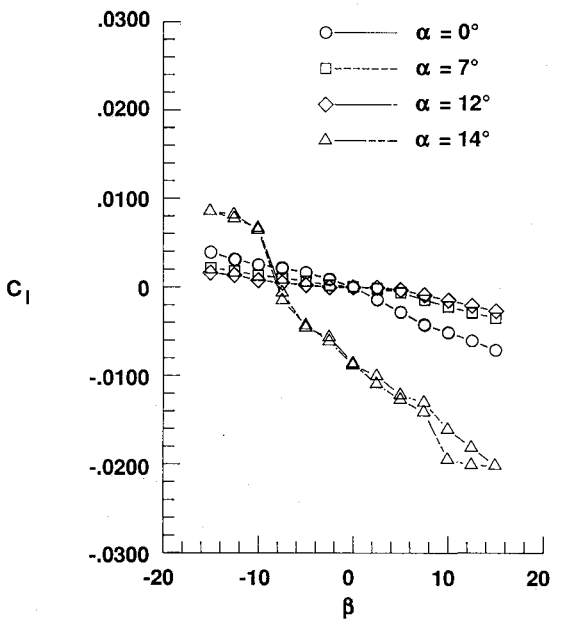

a) Elliptic model

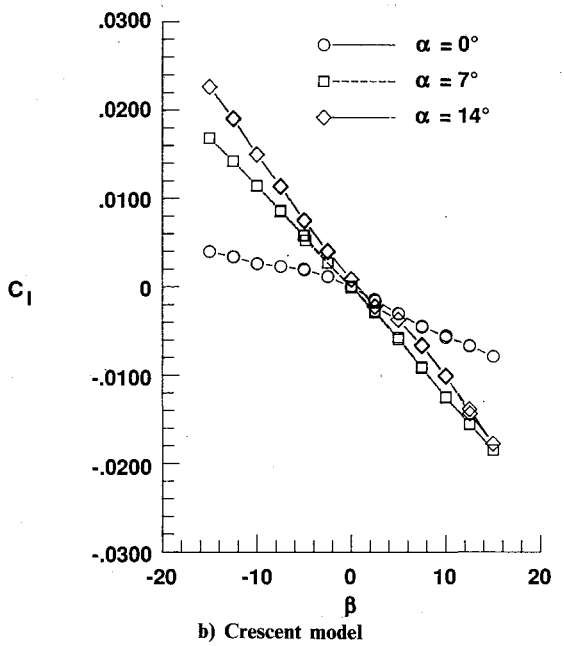

b) Crescent model

Fig. 6 Influence of angle of attack on lateral stability.

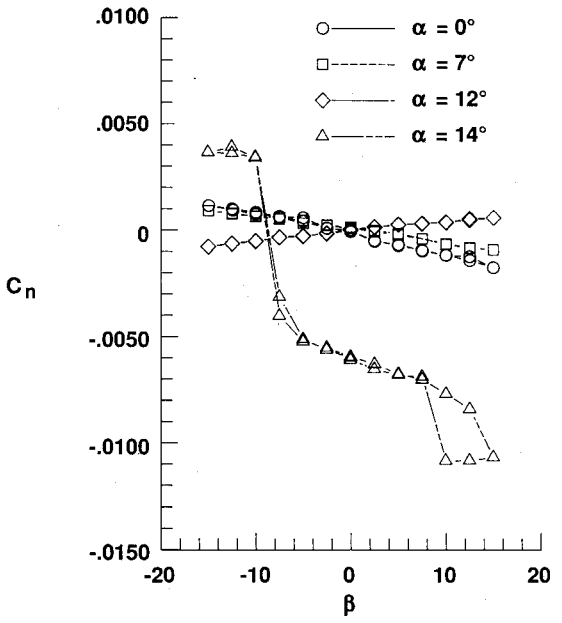

a) Elliptic model

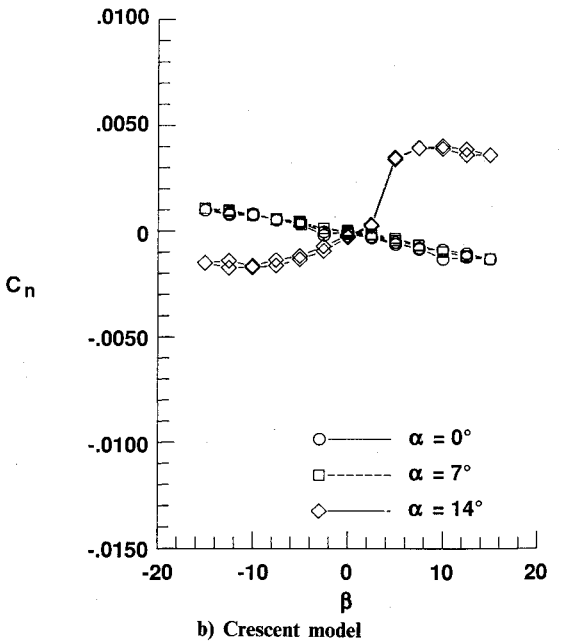

b) Crescent model

Fig. 7 Influence of angle of attack on directional stability.

moment center. The force and moment coefficients were nondimensionalized by the reference wing area of 6.47 ft^2, reference wing span of 6.74 ft, and reference chord (c_{av}) of 0.96 ft.

Forces and Moments

The lift characteristics of the two wings were virtually identical for low angles of attack ($\alpha < 6$ deg), see Fig. 4a. At higher angles of attack, the crescent wing produced slightly less lift for a given incidence angle (Figs. 4a and 4b). A dramatic change occurred at $\alpha = 13$ deg and $C_L = 0.98$. At these test conditions, the elliptic wing reached its maximum lift condition and lift continued to increase for the crescent wing (Fig. 4b). The crescent wing reached a maximum lift coefficient $C_{L,\max} = 1.06$ at $\alpha = 14.5$ deg. The observed poststall behavior of the crescent wing was steady and benign; however, the elliptic wing displayed a much more abrupt and unsteady poststall behavior. This difference in stall and poststall characteristics is shown by the lift data, Fig. 4b. The poststall reductions in lift were nearly linear for the crescent configuration, whereas they were very nonlinear for the elliptic configuration.

The pitching-moment results are presented in Fig. 5. The pitching-moment coefficients for zero angle of attack were identical for both wings. At low angles of attack, the pitching-moment coefficient slope with angle of attack $C_{m,\alpha}$ was about zero for the elliptic wing; i.e., the aerodynamic center was located near the moment center, as expected. The crescent wing displayed a linear and stable $C_{m,\alpha}$ behavior until high angles of attack; $C_{m,\alpha} = -0.014$ deg^{-1} at low angles of attack indicating the location of the aerodynamic center was about $0.18c_{av}$ downstream of the moment center. Nose-down pitching moments were much larger for the crescent wing than for the elliptic throughout the angle-of-attack range, including poststall. This stabilizing effect was expected because of the tendency of the flow to stay attached on the rearward displaced tips of the crescent wing, as will be evident from the flow visualizations.

In Figs. 6 and 7, the lateral-directional results are presented for angles of attack ranging from 0 deg to stall. The rolling-moment coefficient due to sideslip (dihedral effect) exhibited a stable trend for both the elliptic (Fig. 6a) and the crescent model (Fig. 6b). The lateral stability of the elliptic configura-

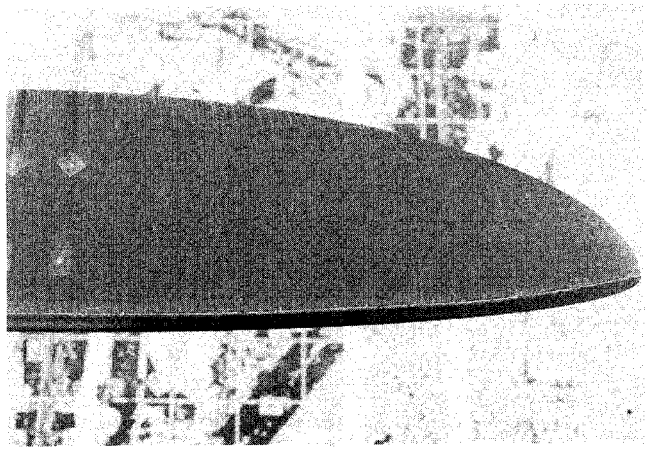

a) $\alpha = 7$ deg

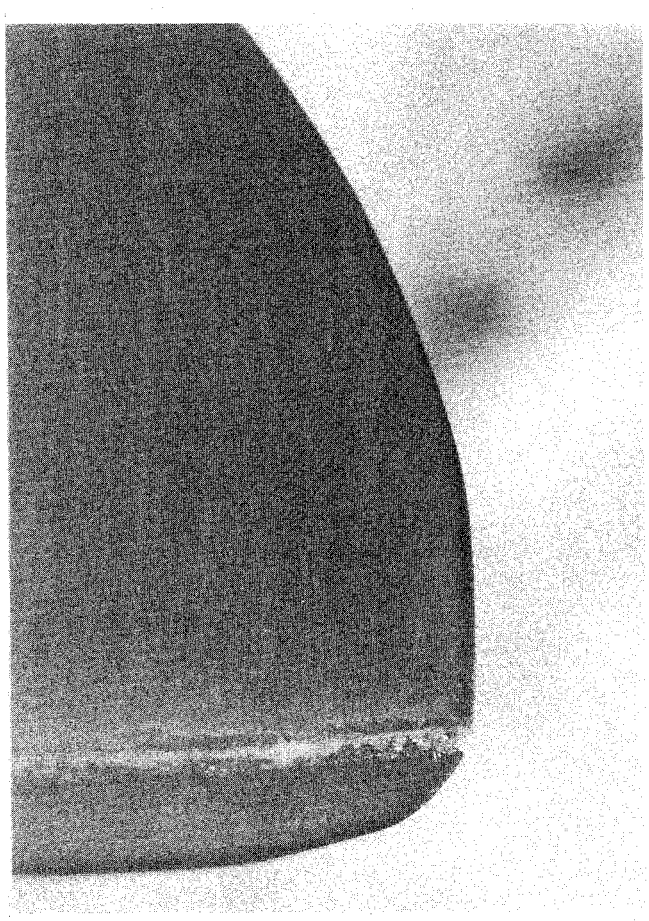

b) $\alpha = 7$ deg

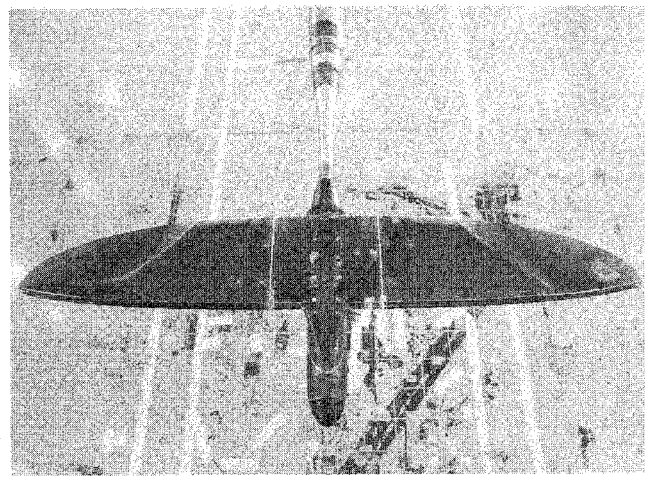

c) $\alpha = 14$ deg

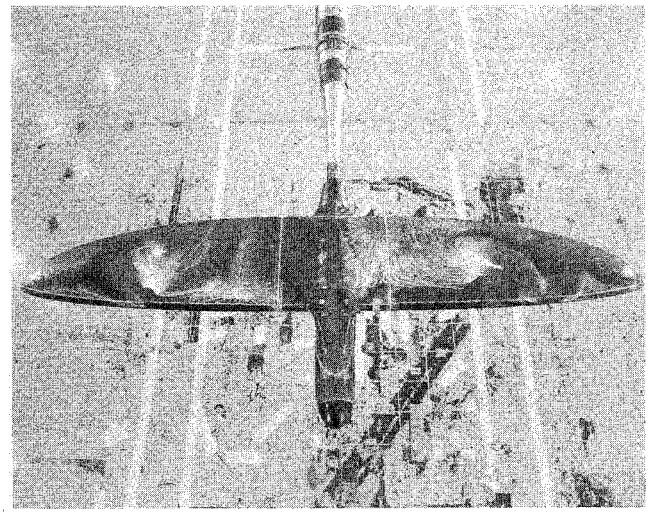

d) $\alpha = 21$ deg

Fig. 8 Titanium-dioxide streak-line patterns over elliptic wing (freestream direction from bottom to top, $\beta = 0$ deg).

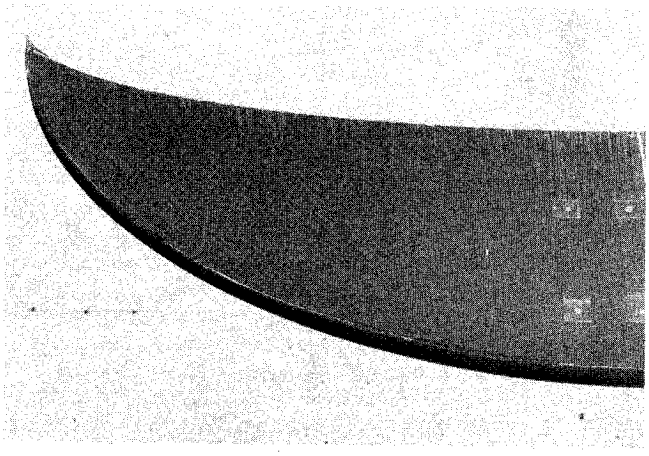

a) $\alpha = 7$ deg

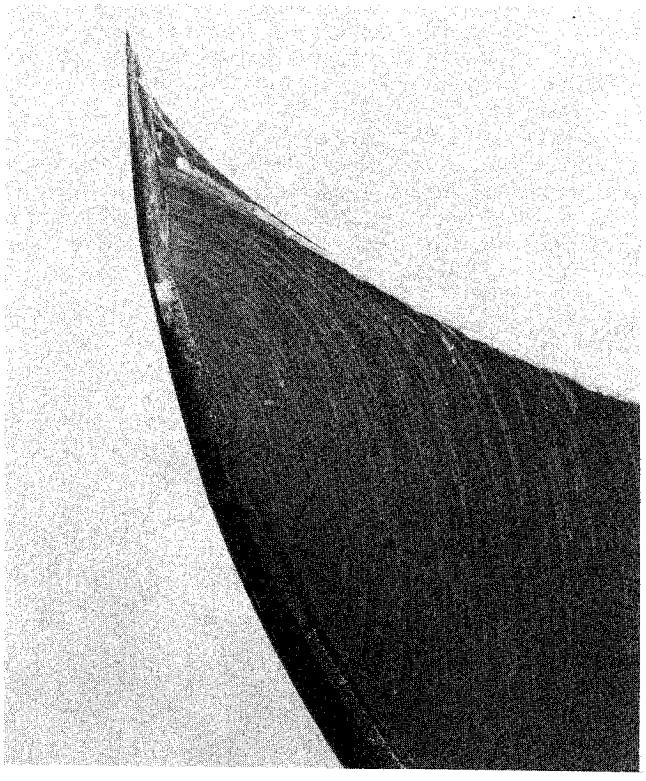

b) $\alpha = 7$ deg

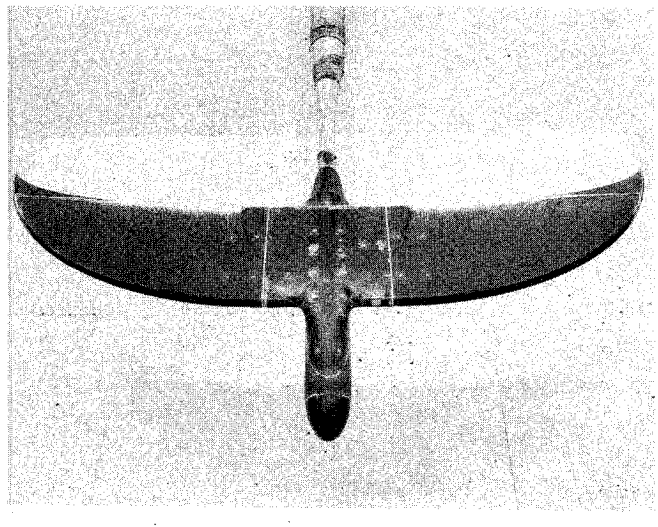

c) $\alpha = 14$ deg

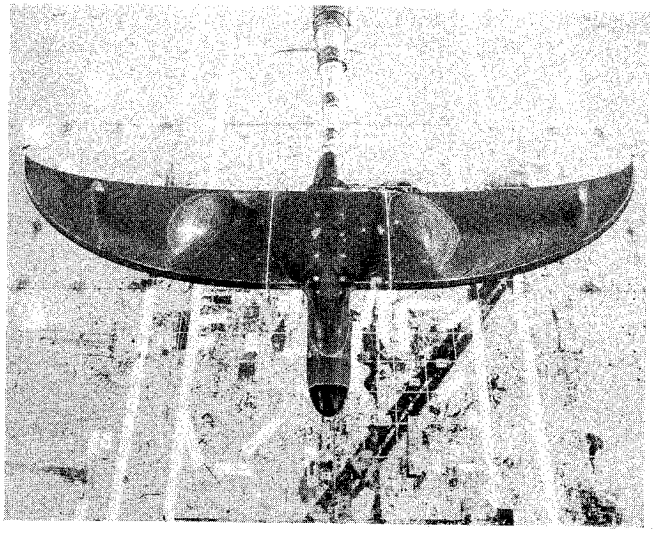

d) $\alpha = 16$ deg

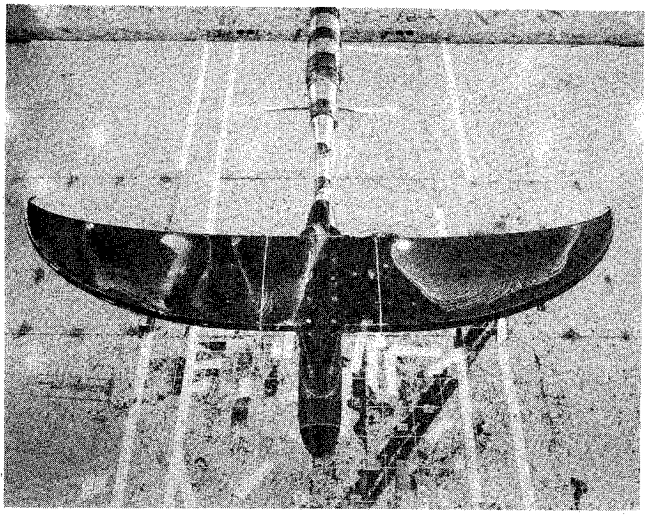

e) $\alpha = 21$ deg

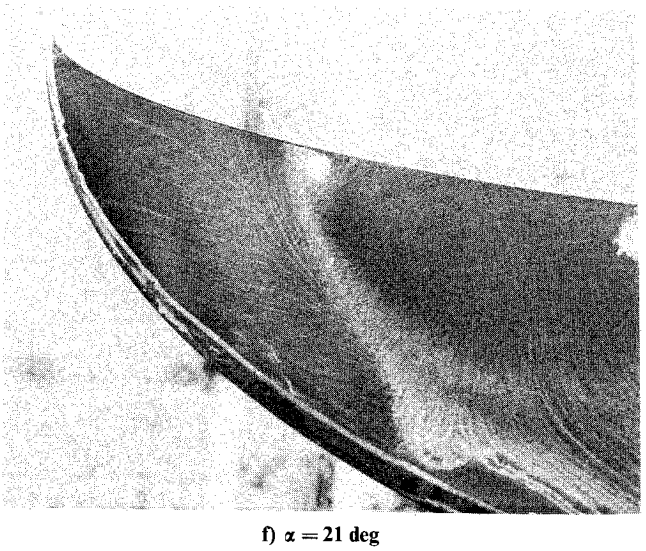

f) $\alpha = 21$ deg

Fig. 9 Titanium-dioxide streak-line patterns over crescent wing (freestream direction from bottom to top, $\beta = 0$ deg).

tion was marginal for incidence angles below stall ($\alpha = 0$, 7, and 12 deg) and pronounced at the poststall condition ($\alpha = 14$ deg). The crescent configuration with the highly swept tips displayed increased lateral stability as compared to the elliptic configuration, as expected.[8] The lateral-directional characteristics of the crescent wing were obtained only at prestall conditions ($\alpha = 0$, 7, and 14 deg).

The yawing-moment coefficient due to sideslip was nearly identical for both wings at low-to-moderate angles of attack (Figs. 7a and 7b). At high but prestall angles of attack, directional stability became positive for both the elliptic (Fig. 7a, $\alpha = 12$ deg) and the crescent model (Fig. 7b, $\alpha = 14$ deg). The crescent configuration, especially, displayed a very stable behavior for small deviations in sideslip angle at this condition. (Note that sizable hysteresis effects were measured for the elliptic wing at poststall conditions.)

Flow Visualizations

Extensive flow-visualization tests on the upper surface (the suction side) of the wings were conducted at various angles of attack. In Figs. 8a and 8b surface-flow patterns in the form of titanium-dioxide streak lines are visible for the elliptic wing at a cruise/climb condition ($\alpha = 7$ deg). The flow pattern over both wing halves was very symmetric; the streak lines ran nearly parallel to the longitudinal axis of the model. No separation or vortex action was detectable in the oil flow pattern near the wingtip at these conditions (Fig. 8b). The results for the crescent wing at the identical conditions are shown in Figs. 9a and 9b. The flow pattern was symmetric, but in the tip region the streak lines displayed a strong outward curvature at this angle of attack. This boundary-layer behavior resulted in limited premature trailing-edge separation at angles of attack above 7 deg and explains the slight reduction in $C_{L,\alpha}$ at those conditions (Fig. 4).

The results for $\alpha = 14$ deg are displayed in Figs. 8c and 9c. The flow over the crescent wing was still attached except for the tip trailing-edge region at this (for the crescent wing) prestall condition (Fig. 9c). However, at this angle of attack, the elliptic wing had stalled and an asymmetric flow pattern had developed (Fig. 8c). A slight variation in the flow angularity across the wind-tunnel test section caused the left wing to stall first. Consequently, the poststall flow patterns remained somewhat asymmetric. In Fig. 8c, the separated flow patterns across the tip regions of the elliptic model are clearly visible. The flow across the inboard portion of the wing was still attached at these conditions. This tip stall appears to explain the abrupt and unsteady behavior of the elliptic wing at these conditions.

At $\alpha \geq 15$ deg, both the elliptic and the crescent model had stalled and displayed asymmetric flow patterns. However, the flow across the elliptic wing was completely separated (Fig. 8d), whereas the tips of the crescent wing exhibited attached flow at these conditions (Figs. 9d–9f). Especially note the vortical patterns across the highly swept wingtips. This vortical flow pattern appears to explain the benign and steady stall behavior of the crescent wing and the increment in lift at stall and poststall conditions, as compared to the unswept elliptic wing.

In Figs. 10 and 11, the surface-flow patterns for both configurations are summarized for $\alpha = 7$, 14, and 21 deg. The streak-line patterns of the attached and separated (reversed-flow) regions were obtained from photographs such as those presented in Figs. 8 and 9 as well as close-up video recordings. Figure 10 clearly depicts the large region of reversed flow over the outboard portion of the elliptic wing at $\alpha = 14$ deg. At $\alpha = 21$ deg, a reversed-flow cell can be observed over the tip region of the elliptic wing. At the same conditions ($\alpha = 21$ deg), a vortical streak-line pattern, with the streak lines oriented approximately parallel to the curved leading edge, occurs outboard of $\eta \simeq 0.75$ for the crescent wing (Fig. 11).

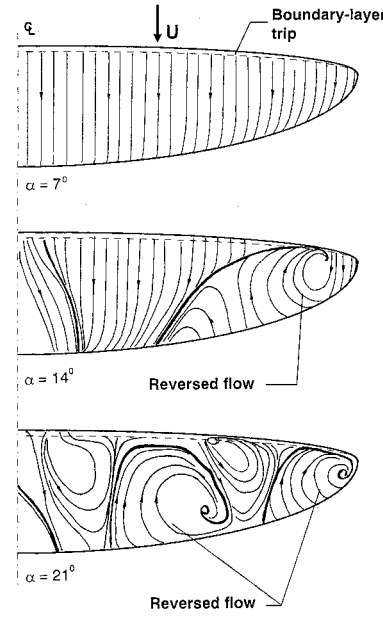

Fig. 10 Summary of surface-flow streak-line patterns over elliptic wing.

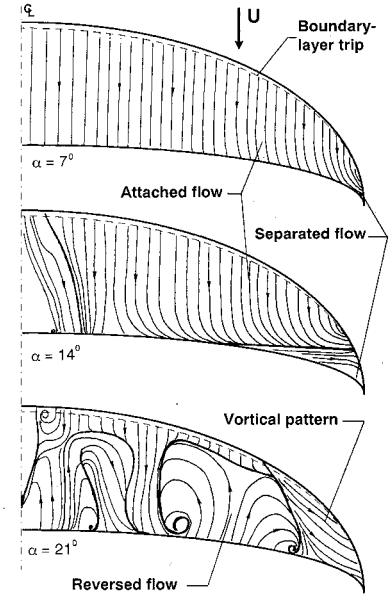

Fig. 11 Summary of surface-flow streak-line patterns over crescent wing.

Concluding Remarks

A low-subsonic wind-tunnel experiment was conducted to explore the differences in high angle-of-attack characteristics of crescent-wing compared to elliptic-wing planforms. On a crescent wing, sweep is used to induce separation along the rounded leading edge of the outboard wing region. The resulting vortical flow over this portion of the wing produces a significant amount of local lift and, therefore, stability and controllability at stall and poststall angles of attack. At cruise and climb conditions, the flow must be kept attached over the entire wing to maximize the leading-edge suction force and, thus, minimize the drag force. This study served to evaluate this concept of combined vortex and attached flows for overall improved wing behavior.

Forces and moments were measured and surface flow visualizations were conducted to compare the aerodynamic characteristics of crescent and elliptic wing planforms at high angles of attack. The wind-tunnel results indicated that the crescent-wing model with its highly swept tips had better high

angle-of-attack aerodynamic characteristics than the unswept elliptic-wing model: 1) $C_{L,max}$ was 8% higher for the crescent wing, 2) poststall lift and pitching-moment behavior was improved for the crescent wing, and 3) prestall dihedral effect of the crescent wing was stronger and more linear than the elliptic wing. The flow visualizations revealed the existence of vortical flow patterns across the highly swept tips of the crescent wing at stall conditions.

These results indicate the potential for improved wingtip aerodynamics by taking advantage of the three-dimensional flow behavior to control separation on surfaces with low tip-chord Reynolds numbers. Also, these experimental results appear to validate the design concept of combining leading-edge separation-induced vortex flows and attached flows for improved behavior for moderate aspect ratio wings at high angles of attack.

More detailed experiments, including surface pressure measurements, are necessary to further explore the static and dynamic aerodynamic characteristics of these wings with highly swept tips at stall and poststall conditions.

Acknowledgments

The work of the first author was supported under NASA Research Grant NAG-1-732 and that of the second author under NASA Contract NAS-1-18240. The authors would like to acknowledge the assistance of the personnel of the 14 × 22 ft subsonic tunnel of the NASA Langley Research Center.

References

[1]Küchemann, D., "On the Possibility of Designing Wings that Combine Vortex Flows with Classical Aerofoil Flows," Royal Aircraft Establishment, Farnborough, Hampshire, England, TM Aero 1363, Oct. 1971.

[2]Küchemann, D., *Aerodynamic Design of Aircraft*, Pergamon, 1978.

[3]"Exploratory Study of the Effects of Wing-Leading-Edge Modifications on the Stall/Spin Behavior of a Light General Aviation Airplane," NASA TP 1589, Dec. 1979.

[4]Robins, A. W., Dollyhigh, S. M., Beissner, F. L., Geiselhart, K., Mertim, G. L., Shields, E. W., Swanson, E. E., Coen, P. G., and Morris, S. J., "Concept Development of a Mach 3.0 High-speed Civil Transport," NASA TM 4058, Sept. 1988.

[5]Wanstall, B., "BERP Blades-Key to the 200 Kn Helicopter," *Interavia*, No. 3, 1986, pp. 322–324.

[6]van Dam, C. P., "Swept Wing-Tip Shapes for Low-Speed Airplanes," Society of Automotive Engineers, Paper 851770, Oct. 1985.

[7]van Dam, C. P., "Aircraft Stall-Spin Entry Deterrent System," U.S. Patent No. 4,776,542, Oct. 1988.

[8]Vijgen, P. M. H. W., van Dam, C. P., and Holmes, B. J., "Sheared Wing-Tip Aerodynamics: Wind-Tunnel and Computational Investigation," *Journal of Aircraft*, Vol. 26, No. 3, 1989, pp. 207–213.

[9]van Dam, C. P., Vijgen, P. M. H. W., and Holmes, B. J., "Wind-Tunnel Investigation on the Effect of the Crescent Planform Shape on Drag," AIAA Paper 90-0300, Jan. 1990.

[10]Holbrook, G. T., Morris Dunham, D., and Greene, G. C., "Vortex Wake Alleviation Studies with a Variable Twist Wing," NASA TP 2442, Nov. 1985.

[11]Henderson, W. P., "Studies of Various Factors Affecting Drag Due to Lift at Subsonic Speeds," NASA TN D-3584, Oct. 1966.

[12]Poll, D. I. A., "Transition in the Infinite Swept Attachment-Line Boundary Layer," *Aeronautical Quarterly*, Vol. 30, Nov. 1979, pp. 607–629.